coatings

MDPI

Review

State of the Art Review on Photocatalytic Fog Seal for Asphalt Pavement: Material Composition, Performance Characterization, Catalytic Mechanism, and Efficacy Enhancement

Zhentong Fan [1], Renjie Zhu [1], Qian Chen [2,*], Futong Xu [1] and Chaozhen Xue [3]

[1] The Second Construction Limited Company of China Construction Eighth Engineering Division, Jinan 250014, China
[2] School of Highway, Chang'an University, Xi'an 710064, China
[3] Shandong Zhongjian Engineering Quality Inspection Co., Ltd., Jinan 250002, China
* Correspondence: 2016121160@chd.edu.cn

Highlights

- Photocatalysts (oxides, nitrides, sulfides) are compared in bandgap, absorption edge, light response, surface area, and solar utilization.
- A three-dimensional indicator framework (efficiency, kinetic, physicochemical) is proposed to explain performance differences from material properties.
- The photocatalytic mechanism and enhancement strategies are summarized, and key design principles for efficiency testing devices are proposed.
- Issues such as lack of testing standards, binder embedding, poor comparability, lab-field gap, and insufficient durability validation are identified.

Abstract

Photocatalytic fog seal technology for asphalt pavement suffers from unclear photocatalyst selection criteria, incomplete testing and evaluation systems, and poorly understood efficacy enhancement mechanisms. This review systematically examines the material composition of photocatalytic fog seals, focusing on photocatalyst types and photoelectric properties. Oxide, nitride, and sulfide photocatalysts are compared in terms of band gap, absorption edge wavelength, photoresponse region, specific surface area, and solar light utilization. Characterization indicators are classified into efficiency, kinetic, and physicochemical categories: efficiency indicators reflect photocatalytic effectiveness, kinetic indicators describe reaction rates, and physicochemical indicators explain intrinsic performance differences. Current testing devices for efficiency indicators are summarized, existing challenges are identified, and essential design features are proposed. The photocatalytic mechanism, including photoexcitation, charge carrier separation, and interfacial catalysis, is elucidated. Performance enhancement strategies—element doping, heterostructure construction, morphology and structure regulation, support loading, and piezo-photocatalytic synergy—are reviewed. Under combined light and mechanical loading, the NO degradation efficiency was 139% and 48% higher than that under pure piezoelectric and pure photocatalytic conditions, respectively. Persistent issues include missing photocatalyst selection standards, neglected binder embedding effects, inconsistent testing methods, poor cross-comparability, laboratory-field

Academic Editor: Carlos Jose Macedo Tavares

Received: 8 October 2026
Revised: 29 October 2026
Accepted: 3 November 2026
Published: 5 November 2026

Copyright: © 2026 by the authors. Licensee MDPI, Basel, Switzerland. This article is an open access article distributed under the terms and conditions of the Creative Commons Attribution (CC BY) license.

discrepancies, and insufficient long-term validation. Accordingly, future research directions and priorities for photocatalytic fog seal technology are identified.

Keywords: road engineering; fog seal; photocatalysis; material composition; performance characterization; efficacy enhancement; mechanism

1. Introduction

Vehicle exhaust is a major source of air pollution; in China alone, motor vehicles emitted 12.856 million tons of pollutants in 2024, of which NOx accounted for 32.30% [1]. The road surface is the initial contact surface for exhaust diffusion [2,3], but conventional road materials are chemically inert and play no role in atmospheric purification. Incorporating photocatalysts into fog seal materials turns this surface into an active degradation interface without additional maintenance, and the resulting photocatalytic fog seal degrades exhaust gases more efficiently than asphalt mixtures containing TiO_2 [4,5].

At the current stage, photocatalytic fog seal technology has progressed beyond the initial proof-of-concept phase toward more advanced directions, including the modification of photocatalytic materials [6–9], carrier optimization [10], and synergistic multi-mechanism efficacy [11]. The photocatalytic carrier has evolved from traditional emulsified asphalt [12,13] to various technical approaches, such as sand-containing fog seals [14,15] and waterborne organic coatings [5,16,17]. Photocatalysts have also diversified from a single type of nano TiO_2 [18,19] to include oxides like CeO_2 [20] and $SrTiO_3$ [21], nitride g-C_3N_4 [22,23], and sulfide $ZnIn_2S_4$ [24], as well as their composite materials [25–28]. Modifications of photocatalysts involve strategies such as metal or nonmetal element doping [29,30], heterostructure construction [31], three-dimensionally ordered macroporous structures [8,32], piezo-photocatalytic composites [11,33], among others [34,35]. For performance evaluation of photocatalytic fog seals, various testing methods, experimental devices, and evaluation indicators have been proposed in existing studies, although their technical focuses differ. Despite this progress, systematic reviews of photocatalytic fog seals are still lacking, and the verification of long-term performance remains largely limited to short-term indoor accelerated aging, so the actual field effectiveness is difficult to assess.

Three issues remain open. First, the performance of a photocatalyst powder is not equivalent to its performance once embedded in the fog seal binder; asphalt films covering the catalyst particles or filling their pores reduce the surface accessible to light and pollutants, and this embedding effect has not been quantified in the existing studies. Second, the efficiencies reported in the literature were obtained with different indicators, test conditions and device configurations, so that the reported results cannot be directly compared across studies. Third, no fog seal binder has so far been designed for photocatalytic function; conventional fog seal materials are directly adopted as carriers without considering their interaction with the photocatalyst.

This review examines the literature on photocatalytic fog seals for asphalt pavements, focusing on three key aspects: material composition, functional properties, and mechanisms of action. It summarizes and analyzes research trends and development directions related to the degradation of road surface exhaust by photocatalytic fog seals. The primary types of photocatalysts used in these fog seals are identified, and the dimensions and categories of functional property indicators are classified. Additionally, the exhaust degradation mechanisms of photocatalytic fog seals are elucidated, and strategies for enhancing their photocatalytic performance are summarized. This review

aims to provide a valuable reference for future research and applications of photocatalytic fog seal technology.

2. Photocatalytic Fog Seal Material Composition

2.1. Carrier Materials

Currently, emulsified asphalt or modified emulsified asphalt is commonly used as the binder material in photocatalytic fog seals. Modified emulsified asphalt is commonly produced with polymer or resin modifiers, whose material composition and technical properties have been reviewed elsewhere [36–40]. Adding nano TiO_2 improves the high-temperature performance of the emulsified asphalt at the cost of its low-temperature performance [41,42]. Thermal oxidative and ultraviolet aging tests indicate an optimal photocatalyst dosage: an appropriate amount of nano TiO_2 enhances the anti-aging performance [43–45], whereas a content exceeding 6% results in a decline [41]. The optimal degradation efficiency of NOx by the photocatalytic fog seal occurs at a nano TiO_2 content of 5%, with cumulative degradation rates of NO and NO_2 reaching 50% and 89%, respectively [14].

The binder determines not only the durability of the seal but also the fraction of catalyst surface that remains accessible. After the emulsified asphalt breaks, the asphalt film anchors the photocatalyst particles onto the road surface and prevents their loss. However, the durability is compromised by mechanical abrasion and the weak bonding within the cementitious system, and traffic and weathering abrasion have been shown to reduce the photocatalytic efficiency [46]. In addition, the active surfaces of the particles may be partially or fully covered by excessive or improperly applied asphalt, with their pores blocked, which hinders light irradiation and pollutant contact. The magnitude of this embedding effect is illustrated by the contrast between incorporation and surface coating: asphalt mixtures modified with 4% TiO_2 in the binder showed an activity below 1%, whereas surface-coated specimens reached an NOx reduction of 22.7% under comparable conditions [4]. In existing studies, binder materials are adopted directly from conventional fog seal practice without targeted selection, and the embedding effect imposed on the photocatalyst by different binder systems, together with its impact on catalytic performance, has been largely overlooked.

2.2. Photocatalysts

At present, the photocatalysts used in fog seals are primarily composed of oxides, sulfides, nitrides, and novel nanomaterials. Although all types of photocatalysts share the fundamental mechanisms of light absorption, charge separation, and surface reactions, their band structures, stability, and application focuses differ significantly due to the intrinsic properties of the materials.

2.2.1. Oxides

(1) TiO_2

Anatase and rutile TiO_2 are the most extensively employed photocatalysts in the field and are commonly used in photocatalytic fog seals. These two phases exhibit different surface energies and reactivities due to their distinct atomic arrangements on the crystal facets. Compared to the rutile phase (~3.0 eV), the anatase phase (~3.2 eV) of TiO_2 possesses a higher conduction band position, faster electron migration rate, and slower electron-hole recombination rate, resulting in higher catalytic activity [47]. TiO_2 is characterized by exceptional chemical stability, resistance to photocorrosion, nontoxicity, and low cost—advantages that are difficult to match with other novel materials. TiO_2 is a wide band gap semiconductor (Eg = 3.2 eV for anatase) and can therefore absorb only light

of wavelength shorter than 387 nm. The ultraviolet portion of the AM1.5G spectrum below this wavelength carries approximately 4% of the total irradiance, and the apparent quantum efficiency of TiO_2 under ultraviolet irradiation does not exceed 28%; the fraction of solar energy actually converted is therefore about 1%, obtained as the product of the two quantities. The 4% value listed in Table 1 refers to the former quantity and should not be read as a conversion efficiency [48,49]. Additionally, TiO_2 suffers from rapid recombination of photogenerated carriers, which limits the purification efficiency per photon [50].

Table 1. Optical properties of photocatalysts currently used for fog seals.

Photocatalyst	Band Gap/eV	Absorption Edge Wavelength/nm	Photoresponse Region	Specific Surface Area/(m^2/g)	Solar Light Utilization Efficiency
TiO_2	3.2 (anatase phase)	≤387	ultraviolet light	up to 213	about 4%
CeO_2	2.9~3.2	384~420	ultraviolet light	22~121	4%~6%
g-C_3N_4	about 2.7	≤460	visible light,	about 10	significantly higher
$ZnIn_2S_4$	2.06~2.85	435~602	visible light,	11~98	than that of TiO_2
$SrTiO_3$	3.2~3.4	365~387	Ultraviolet light	/	about 4%

(2) CeO_2

Cerium dioxide, a rare earth metal oxide with unique reversible redox properties, is characterized by a cubic fluorite crystal structure [21]. The formation of oxygen vacancies enables the partial reduction in Ce^{4+} to Ce^{3+} and confers the distinctive redox capability through the variable valence states of cerium (Ce^{3+}/Ce^{4+}) [51–53]. Nanoceria exhibits a high specific surface area, 48.8 m^2/g for the material studied in [54], with a significant surface site concentration (edge sites 0.177 mol/kg, layer sites 0.228 mol/kg); values between 22~121 m^2/g have been reported for ceria powders of different origin. As a unique lanthanide oxide, CeO_2 possesses favorable redox properties due to the variable valence states of cerium, which can exist as Ce^{3+} or Ce^{4+} through electron transfer [52,53]. The absorption onset of CeO_2 lies between 384 and 420 nm, extending beyond that of anatase TiO_2 to the boundary of the ultraviolet region. The band gap reported for ceria varies from 2.9 to 3.2 eV, the lower values being associated with a higher Ce^{3+} content and hence a higher oxygen-vacancy concentration; since the redox behaviour discussed above depends on the same defect population, a single band gap value should not be assigned without specifying the defect state [21,51–53]. Moreover, studies have demonstrated that the photocatalytic NO degradation capability of nano-CeO_2 surpasses that of nano-TiO_2 [21].

(3) Strontium titanate

Nano-sized $SrTiO_3$ is characterized by a relatively stable cubic perovskite-type crystal structure and strong corrosion resistance [55]. Its structural framework is formed by tightly bonded corner-sharing TiO_2 octahedral units, which constitute the lattice skeleton [56]. Both the crystal structure and photocatalytic activity of $SrTiO_3$ are more stable than those of TiO_2 [57]. The band gap of $SrTiO_3$ ranges from 3.2 to 3.4 eV, so that charge carriers are generated only under ultraviolet light with a wavelength shorter than 365~387 nm. The fraction of the AM1.5G spectrum accessible to the material is accordingly about 4%, comparable to that of anatase TiO_2.

Cation substitution at the Sr^{2+} and Ti^{4+} sites generates anion defects and oxygen vacancies, thereby enhancing the photocatalytic activity without altering the crystal structure [21]. Experimental evidence has demonstrated that the catalytic NO degradation performance of nano $SrTiO_3$ surpasses that of nano TiO_2 [21].

2.2.2. Nitrides

At present, the nitride photocatalyst primarily used in fog seals is g-C_3N_4. Among the various phases of C_3N_4, g-C_3N_4 exhibits the most stable chemical properties. Graphitic carbon nitride (g-C_3N_4) is a stable layered structure composed of carbon and nitrogen atoms covalently bonded together. Each stacked layer consists of s-triazine (C_3N_3) units, with the layers held together by weak van der Waals forces. This layered structure provides a large accessible surface area after exfoliation, although the bulk material typically exhibits only about 10 m^2/g, which still offers sufficient sites for reactant adsorption and photocatalytic reactions [58,59]. g-C_3N_4 possesses a tunable band gap and abundant active sites [60,61]. Similar to TiO_2, a high recombination rate of electrons and holes significantly limits the photocatalytic activity of g-C_3N_4 [61,62]. Compared to traditional wide-bandgap TiO_2, g-C_3N_4 has a narrower band gap of about 2.7 eV [63] and an absorption edge near 460 nm, so that a larger fraction of the AM1.5G spectrum lies above the gap; the utilization of about 10% quoted in [64] is close to this spectral fraction [60]. Its photocatalytic efficiency is nevertheless lower than that of TiO_2, which is attributable to the rapid recombination of photogenerated carriers rather than to the optical absorption [61,62].

2.2.3. Sulfides

Among ternary sulfide semiconductors, $ZnIn_2S_4$ is one of the few photocatalysts with a layered structure. It exhibits a tunable band gap ranging from 2.06 to 2.85 eV and demonstrates favorable photocatalytic performance within the visible light response region [65]. The distinctive petal-like spherical nanosheet layered structure of $ZnIn_2S_4$ provides a specific surface area of 58.4 m^2/g [66], within the 11~98 m^2/g range reported for this system, supplying abundant reactive sites for photocatalytic reactions. The layered structure allows $ZnIn_2S_4$ to be readily coupled with other semiconductors, such as the $TiO_2/ZnIn_2S_4$ heterojunction formed via a hydrothermal method [67–69]. $ZnIn_2S_4$ exists in three crystal structures. The hexagonal phase exhibits superior photocatalytic performance. The cubic and hexagonal phases show absorption wavelengths of 538 nm and 490 nm, respectively, with corresponding band gaps of 2.3 eV and 2.5 eV [68,70]. However, photocorrosion of metal sulfides is primarily induced by the interaction between photogenerated holes and the surrounding medium, which directly degrades their morphology, structure, and surface chemical composition [71], thereby resulting in a pronounced loss of photocatalytic activity and service life.

2.2.4. Comparison of Photocatalysts

Although various photocatalysts for fog seals, including metal oxides, nitrides, and sulfides, have been reported in the literature, most existing studies have focused primarily on verifying the efficacy of single-material systems. Insufficient attention has been given to cross-comparisons of the optical properties among different material categories. This research paradigm, which emphasizes application while neglecting comparative analysis, leads to a lack of screening criteria and structure-activity relationships when selecting photocatalysts under specific carrier and service environment constraints. Consequently, this results in inefficiency and a lack of direction in material selection. Therefore, the optical properties of photocatalysts currently used for fog seals are systematically summarized in Table 1.

2.3. Stabilizers

Due to the higher relative density of the photocatalyst compared to that of the fog seal binder material, poor compatibility often occurs between the two, leading to segregation issues that adversely affect photocatalytic performance. TiO_2 powders also

tend to agglomerate and settle out of the emulsion before spraying, which reduces the uniformity of the catalyst distribution on the pavement surface [72]. To mitigate this, stabilizers are commonly introduced during the preparation of photocatalytic fog seal materials to reduce the sedimentation velocity of photocatalyst particles within the binder. Stabilizers are generally classified into inorganic and organic types. Inorganic stabilizers enhance the electrical double layer effect and increase the zeta potential around emulsion particles, thereby strengthening the mutual repulsive forces between particles and reducing coagulation rates. Common inorganic stabilizers include sodium hexametaphosphate [13], calcium chloride [32,41], ammonium chloride [73], and magnesium chloride [73]. Generally, organic stabilizers exhibit superior stabilizing effects compared to inorganic ones. Examples include sodium carboxymethyl cellulose [32] and polyvinyl alcohol [8]. The dosage of stabilizers is typically controlled within 5% of the mass fraction of the emulsified asphalt [13,74]. However, existing research on photocatalytic fog seals primarily employs stabilizers as auxiliary agents to improve storage stability, often neglecting their influence on photocatalytic performance. Moreover, comparative studies examining the effects of different stabilizers on both system stability and photocatalytic efficiency remain limited, and targeted investigations into the compatibility between various photocatalysts and emulsified asphalt are scarce.

3. Action Mechanism of Photocatalytic Fog Seal

When ultraviolet or visible light with a wavelength shorter than a specific threshold irradiates a semiconductor material (photocatalyst), energy exceeding its band gap is absorbed, exciting electrons from the valence band to the conduction band under the influence of the internal electric field. These excited electrons subsequently migrate to the particle surface. Simultaneously, an equal number of positively charged holes are generated in the valence band, forming electron-hole pairs (photogenerated charge carriers). These pairs rapidly separate and migrate to the photocatalyst surface. The high-energy electrons at the surface exhibit strong reducing power and readily react with oxygen molecules adsorbed on the surface, producing superoxide radicals ($\cdot O_2^-$). Meanwhile, the holes possess strong oxidizing ability and extract electrons from adsorbed water molecules, generating hydroxyl radicals (·OH) [75]. Both superoxide and hydroxyl radicals are highly reactive oxidants that engage in redox reactions with harmful gases such as CO, hydrocarbons (HC), and NOx adsorbed on the photocatalyst surface, converting them into CO_2, H_2O, and nitrate species. However, electron-hole pairs are prone to recombination after photoexcitation, releasing energy as heat and other forms, which diminishes the photocatalytic efficiency. Consequently, only a fraction of the non-recombined electron-hole pairs reach the semiconductor surface to participate in redox reactions. The mechanism of exhaust gas degradation by nano TiO_2 photocatalysis is illustrated in ref. [40].

The photocatalytic process can be divided into three stages: light absorption, charge separation and migration, and surface catalytic reactions.

The reaction equation for light absorption is given in Equation (1).

$$M + hv \rightarrow h^+ + e^- \quad (1)$$

The reaction equations for charge separation and migration is given in Equations (2) and (3).

$$h^+ + H_2O \rightarrow \cdot OH + H^+ \quad (2)$$

$$e^- + O_2 \rightarrow \cdot O_2^- \quad (3)$$

The reaction equations for surface catalytic reactions is given in Equations (4)–(8).

$$NO + \cdot O_2 \rightarrow NO_3^- \quad (4)$$

$$NO_2 + \cdot OH \rightarrow NO_3^- + H^+ \quad (5)$$

$$HC + O_2 \rightarrow CO_2 + H_2O \quad (6)$$

$$CO + \cdot OH \rightarrow CO_2 + H + {}^+ e^- \quad (7)$$

$$CO + h^+ \rightarrow CO^{+\cdot} \rightarrow CO_2 \quad (8)$$

4. Evaluation Methodology for Photocatalytic Fog Seal Performance

4.1. Indicator System for Performance Characterization

At the current stage, numerous indicators are used to evaluate the catalytic performance of photocatalytic fog seals. Based on differences in evaluation scales, these indicators can be classified into three categories: physicochemical indicators, kinetic indicators, and efficiency indicators, as illustrated in Figure 1. These categories do not exist independently; rather, they form a complete causal chain from the macroscopic to the microscopic level and from observable phenomena to underlying essence. Specifically, the intrinsic mechanism driving the photocatalytic effect of the fog seal is represented by physicochemical properties, the intermediate processes are described by kinetic performance, and the ultimate macroscopic outcomes are reflected by efficiency indicators.

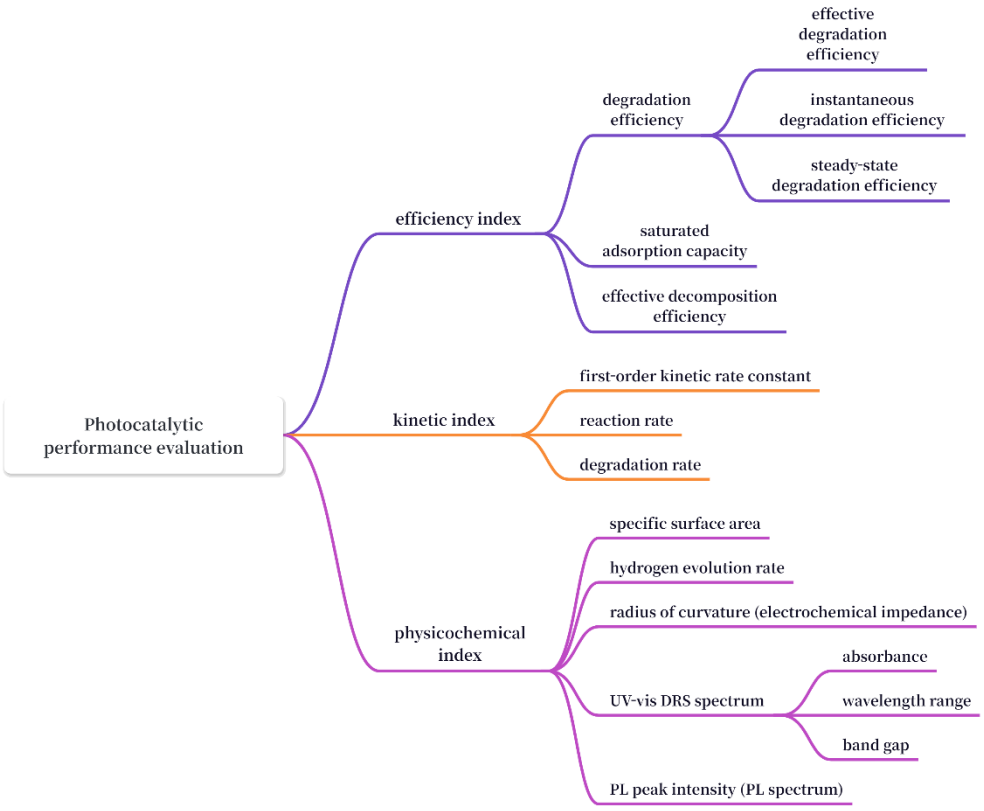


Figure 1. Evaluation indicator map for the photocatalytic performance of fog seals [5,9,10,14,21,24,32,33,76–80].

4.1.1. Efficiency Indicators

Efficiency indicators are used to measure the effectiveness of photocatalytic reactions in fog seals and are considered the most important evaluation criteria. Currently, the primary efficiency indicators for assessing the purification performance of photocatalytic fog seals include degradation efficiency, saturated adsorption capacity, and effective decomposition efficiency.

(1) Degradation efficiency

Degradation efficiency (or degradation effectiveness) is defined as the percentage reduction in exhaust gas concentration achieved by the photocatalytic fog seal within a specified time period, as shown in Equation (9). Depending on the duration considered, degradation efficiency is further categorized into instantaneous degradation efficiency and stable degradation efficiency. To account for the natural concentration loss of the gas itself, the concept of effective degradation efficiency was introduced [77]. This is defined as the actual effective concentration reduction rate of component x in the experimental group within time t, after eliminating the influence of the blank group, as shown in Equation (10). In practice, the degradation efficiency has been monitored continuously with an NO_2 concentration probe [9] or determined by spectrophotometry of the absorption solution according to HJ 479-2009.

$$\kappa = \frac{\rho_{\max} - \rho_{\min}}{\rho_{\max}} \times 100\% \tag{9}$$

where $\rho_{\max}$ is the maximum initial gas concentration, $\rho_{\min}$ is the minimum gas mass concentration after stabilization.

$$P_{e,t,x} = \frac{P_{m,t,x} - P_{b,t,x}}{1 - P_{b,t,x}} \tag{10}$$

where, $P_{m,t,x}$ is the measured exhaust degradation rate, the reduction rate of the concentration of component x obtained in the experimental group within time t; $P_{b,t,x}$ is the background exhaust loss rate, the reduction rate of the concentration of component x in the blank group within time *t*; $P_{e,t,x}$ is the effective exhaust degradation rate, the actual effective concentration reduction rate of component x in the experimental group within time t after the influence of the blank group is eliminated.

(2) Effective decomposition efficiency and saturated adsorption capacity

The catalyst mass was included in the evaluation scope. The effective decomposition efficiency and saturated adsorption capacity were proposed as key metrics [79,80]. The photocatalytic performance of the fog seal was measured by the mass of exhaust gas degraded per unit mass of catalyst or fog seal, as shown in Equations (11) and (12), respectively. Compared to degradation efficiency alone, the relationship between exhaust degradation efficiency and dosage is more directly reflected by the effective decomposition efficiency and saturated adsorption capacity. These metrics provide objective and highly comparable data, effectively meeting practical engineering requirements. However, these two indicators do not account for variations in the initial exhaust concentration, which may lead to an overestimation of the degradation effect for high-concentration exhaust.

$$\eta = \frac{(C - C_P) \times V \times \rho}{m_P} \tag{11}$$

where η is the effective decomposition efficiency, m_P is the mass of the photocatalyst, V is the volume of the harmful gas, ϱ is the density of the harmful gas, C and C_P are the concentrations of the harmful gas before and after the addition of the photocatalyst, respectively.

$$q = (C_0 - C_e) \times \frac{V}{m} \tag{12}$$

where q is the saturated adsorption capacity, m/g; C_0 is the initial concentration, mg/L; C_e is the equilibrium concentration, mg/L; V is the gas volume, L; m is the mass of the fog seal, g.

Current efficiency indicators for evaluating the catalytic effectiveness of fog seals do not simultaneously consider both conversion and selectivity. Existing studies primarily focus on the concentration changes in harmful gases such as CO, NOx, and HC, while neglecting their redox products. Specifically, it remains unclear whether CO, HC, and NOx are converted into the desired target products after the redox reactions, whether incomplete redox occurs, or whether other harmful byproducts are generated. For example, NO may be excessively oxidized to NO_2.

4.1.2. Kinetic Indicators

Kinetic indicators are used to elucidate the intrinsic mechanisms and rate-controlling steps of catalytic reduction reactions. Currently, the characterization metrics for the degradation performance of photocatalytic fog seals include the first-order kinetic rate constant, the overall reaction rate, and the degradation rate.

(1) First-order kinetic rate constant

The rate constant can be readily determined by measuring pollutant concentrations at different time points and plotting the curve of $ln(C_0/C_t)$ versus time (t). The value of k is obtained as the slope of the linear fit, allowing for an objective quantification of exhaust degradation efficiency under various catalysts and reaction conditions, as shown in Equation (13) [33]. It is particularly applicable to low-concentration systems, consistent with the actual concentrations found in vehicle exhaust. However, the rate constant is an apparent constant that encompasses the contributions of multiple processes, thereby neglecting the complexity of the reaction mechanism. In a photocatalytic reaction with a high rate constant, this may result from a strong surface reaction capability of the catalyst, a high adsorption capacity, or both. Consequently, the underlying reason for the performance enhancement cannot be directly determined.

$$k = \frac{\ln(C_0 / C_t)}{t} \tag{13}$$

where C_0 and C_t are the initial and instantaneous concentrations of the exhaust gas, respectively; k is the first-order kinetic rate constant.

(2) Overall reaction rate and degradation rate

In contrast to degradation efficiency, the effect of reaction time is reflected in the overall reaction rate and the degradation rate, which represent the decrease in the target gas concentration per unit time [79], as shown in Equations (14) and (15), respectively. The overall reaction rate is influenced by factors such as catalyst dosage, light intensity, initial reactant concentration, reaction temperature, physical properties of the reactants, and gaseous oxygen concentration. The degradation rate represents the average rate at which the target gas concentration decreases over a given time period, whereas the overall reaction rate corresponds to the instantaneous rate of decrease in the target gas. Typically,

a high degradation efficiency results from a high reaction rate achieved within a shorter reaction time.

$$r = -\frac{dC_s}{dt} = \frac{k_r K C_s}{(1 + K C_s)} \tag{14}$$

where r is the overall reaction rate of the reactant, mg/(m³·min); C_s is the concentration of the reactant, mg/m³; t is the reaction time, min; k_r is the reaction rate constant of the reactant, min⁻¹; K is the adsorption constant of the reactant on the catalyst.

$$\eta' = \frac{C_0 - C_1}{t} \tag{15}$$

where η' is the degradation rate.

The first-order kinetic rate constant, overall reaction rate, and degradation rate reflect only the disappearance rate of the target gas. They do not provide information on intermediate or final products, which may pose new potential environmental risks.

4.1.3. Physicochemical Indicators

The differences in the catalytic effectiveness of photocatalytic fog seals can be attributed to various physicochemical factors. Currently, the key physicochemical indicators used to evaluate the photocatalytic performance of fog seals include specific surface area, morphology and structure, electrochemical impedance, hydrogen evolution rate, and spectral range, among others.

(1) Specific surface area and morphology and structure

A larger specific surface area implies a greater number of active sites, which provide locations for reactant adsorption and surface reactions [28]. Increasing the contact area between the photocatalyst and pollutant gases, as well as the number of catalytically active sites, is generally achieved through morphology and structural regulation, thereby enhancing degradation performance.

(2) Electrochemical impedance

Electrochemical impedance reflects the efficiency and resistance of charge separation and transport. In electrochemical impedance spectroscopy (EIS), the interfacial resistance between the electrolyte and the electrode is represented by the radius of the semicircular curve. A smaller radius indicates lower resistance to electron migration. This lower resistance facilitates faster separation of photogenerated electrons and holes, accelerating interfacial charge transfer. Consequently, the interfacial reaction kinetics are enhanced, significantly improving photocatalytic activity.

(3) UV vis DRS and PL spectroscopy

The light absorption behavior of a photocatalyst at different wavelengths—specifically its absorbance and photoresponse range—is primarily characterized by Ultraviolet-Visible (UV-Vis) diffuse reflectance spectroscopy (DRS). Higher absorbance indicates a greater potential for capturing more photons and generating more charge carriers (electrons and holes), thereby enhancing catalytic activity. An ideal photocatalyst should exhibit strong and broad absorption within the target spectral range. The longest wavelength boundary of the light that can be absorbed is directly determined by the band gap energy (Eg) of the photocatalyst; their relationship is expressed in Equation (16). To absorb visible light with wavelengths longer than 400 nm, the band gap of a photocatalyst must be adjusted to below 3.1 eV; however, pure nano TiO_2 exhibits a band gap of 3.2 eV.

$$E_g = h \times c / \lambda \quad (16)$$

where λ is the absorption edge, nm; E_g is the band gap energy, eV; h is the Planck constant, h=6.626×10^{-34} J·s; c is the speed of light, c=2.998×10^{8} m/s.

Photoluminescence (PL) spectroscopy is used to analyze the recombination process of photogenerated electron-hole pairs [6]. A low PL intensity indicates suppressed recombination and hence higher catalytic activity, whereas a high intensity corresponds to low activity. After introducing 3% CNT, the photoluminescence intensity of ZIS significantly decreases, indicating that the recombination efficiency of photogenerated electrons and holes within the material is greatly reduced [24].

The physicochemical indicators explain the origin of performance, the kinetic indicators reflect the degradation rate, and the efficiency indicators describe only the net outcome. A favorable band gap or strong photoluminescence quenching does not guarantee a large rate constant, because the apparent rate constant also absorbs the contributions of adsorption, mass transfer, and light intensity. Conversely, a large rate constant does not ensure a high degradation efficiency, since the efficiency depends strongly on the initial concentration and the test duration, whereas the rate constant is approximately independent of them under pseudo-first-order conditions. Therefore, these indicators should be used in a combined manner with clearly reported test conditions. The physicochemical indicators are suited to material screening and quality control, the rate constant is suited to rate comparison across conditions under pseudo-first-order assumptions, and the efficiency indicators are suited to horizontal comparison within the same apparatus.

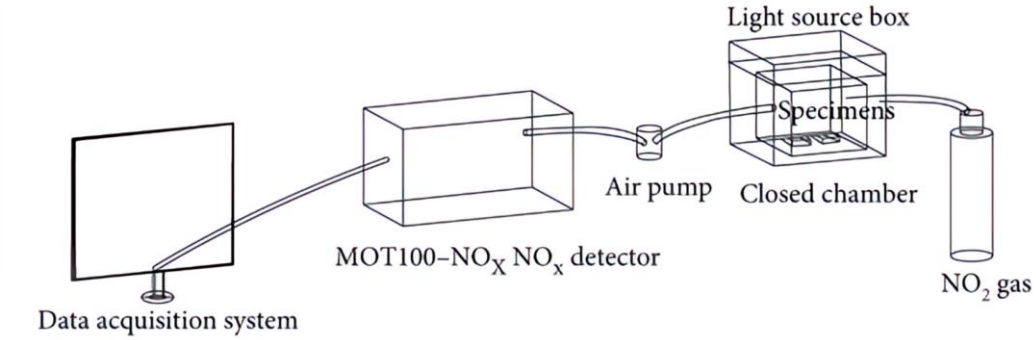
4.2. Testing Methods and Devices

At the present stage, testing devices for the physicochemical and kinetic indicators of photocatalysts are relatively well established, and the corresponding testing methods are fairly mature. Various devices have been used to measure the efficiency indicators, as shown in Table 2. Some representative testing devices are shown in Figure 2. Unified standards regarding structure, light source, and reaction condition control are lacking, which compromises the comparability of experimental data across different studies and consequently affects the objective evaluation of the degradation performance of photocatalytic fog seals.

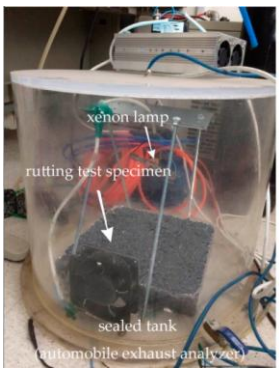
Table 2. Statistics of testing devices for photocatalytic performance of fog seals at the present stage.

Literature Source	Reactor Type and Volume	Light Source Type and Intensity	Target Gas and Initial Concentration	Specimen Substrate	Testing Frequency	Characterization Indicator
Yan et al. [81]	Static batch, 100 L	10 W Ultraviolet lamp, 30 W/m^2	NOx 105 mg/m^3 CO 8880 mg/m^3 SO_2 568 mg/m^3	Asphalt mixture slab specimen, 30 cm × 30 cm × 5 cm	10 min/time	Maximum degradation rate, degradation effectiveness
Guo et al. [82]	Static batch, 43.32 L	Simulated daylight lamp	5260 ppm HC, 12,623 ppm NO		5 min/time	Degradation effectiveness, 30 min average degradation rate
Shan [77]. Zhang et al. [7]	Dynamic flow, 120 L	Ultraviolet lamp	317.5 ppmCO, 4.8 ppm NO, 3.3 ppm NO_2		5 min/time + 10 min/time	Effective degradation rate

Wang [78]	Static batch, 51.3 L	Ultraviolet lamp	5%CO, 10%NOx	Asphalt mixture slab specimen, 35 cm × 35 cm × 5 cm	30 min/time	Instantaneous degradation rate, cumulative degradation rate
Zhang [24]	Static batch, 51.3 L	Ultraviolet lamp	NOx 25~26 ppm vol	Asphalt mixture slab specimen, 30 cm × 30 cm × 5 cm	1 min/time	Instantaneous degradation rate, average degradation rate
Wang [79] Xu et al. [8]	Static batch	Ultraviolet lamp 30 W/m^2	1 mg/L NO		1 min/time	Steady-state degradation rate
Li et al. [50]	Static batch, 100 L	Ultraviolet lamp, 300 W/m^2	20 ppm NO_2	Asphalt mixture slab specimen, 15 cm × 15 cm × 5 cm	30 min/time	Degradation efficiency
Zhang et al. [80]	Static batch	Ultraviolet lamp, 8.88~52.24 W/m^2	CO 0.47% vol, NO 194 × 10^{-6} ppm, HC 99 × 10^{-6} ppm	Asphalt mixture slab specimen, 30 cm × 30 cm × 5 cm	/	Cumulative decomposition rate, effective decomposition rate
Yuan [83]	Static batch, 676 L	Ultraviolet lamp	NOx 1500 ppb, CO 15%		1 min/time	Degradation effectiveness
Li [84]	Static batch, 27 L	Ultraviolet lamp, 25.0 W/m^2	HC 195 ppm CO 1.55%vol NO 225 ppm		5 min/time	Cumulative decomposition rate

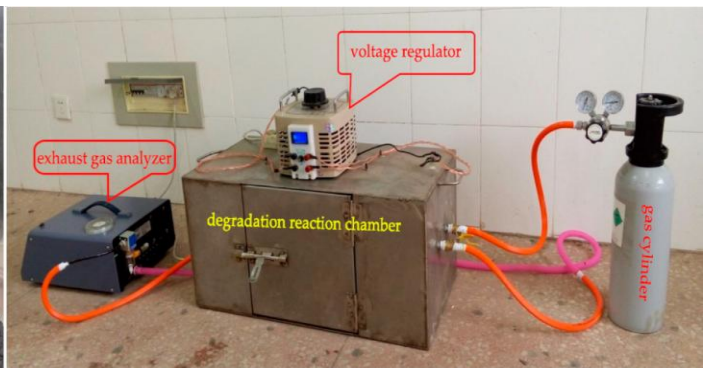


(**a**)



(**b**)





(**c**)

Figure 2. The testing device for the degradation performance of photocatalytic fog seals. (**a**) [50]. (**b**) [85]. (**c**) [86].

In current research on the degradation performance of photocatalytic fog seals, independently developed testing devices are predominantly used. As a result, key test parameters—such as reactor dimensions, light source wavelength, and gas flow rate—vary significantly, making it difficult to compare performance data across different research groups. Although these testing devices differ in design, they essentially function as ideal environmental reactors at the laboratory scale and primarily consist of three components: a gas supply system, a reaction system, and a testing system.

(1) Gas supply system

In existing studies on photocatalytic fog seals, cylinders containing simulated gases are commonly used as the gas supply system. The minimum gas concentration in these cylinders is typically 10 ppm. If the gas concentration from the cylinders is directly adopted, it can create a misleading impression of inflated degradation efficiency. An ideal gas supply system consists of standard gas cylinders (CO, HC, NOx), zero-grade air and flow controllers, so that the initial concentration of the target gas can be set to match roadside conditions.

An ideal gas supply system should consist of gas cylinders (CO, HC, NOx), an air compressor or flow controller, and a gas mixing chamber. The reaction gas is prepared by mixing a standard target gas with zero-grade air. The target gas is introduced into the reaction system at a specified concentration, and the flow rate of the reaction gas and the concentration of the target gas are controlled by separately adjusting the air and the standard target gas via flow controllers. After mixing zero-grade air and the standard target gas, the mixture is introduced into the reaction chamber.

The concentration of the target gas should closely match practical conditions, as higher degradation efficiency tends to be observed with increasing initial exhaust concentrations [87]. If the initial exhaust concentration range in laboratory tests deviates significantly from actual conditions, the true degradation performance of the photocatalytic fog seal cannot be accurately reflected. The NO concentration in motor vehicle exhaust is generally below 1 ppm [4,21]. Therefore, the initial NO concentration in laboratory tests should be controlled within the range of 0.5 to 1.0 ppm [21].

(2) Reaction system

Studies have demonstrated a nonlinear, binary increase in the photocatalytic performance of fog seals with rising light intensity. When the UV light intensity increases from 8.88 W/m^2 to 34.8 W/m^2, the cumulative decomposition rates of CO, HC, and NO increase by 145.20%, 112.45%, and 111.27%, respectively [80]. Ambient temperature effectively enhances the photocatalytic performance of the fog seal. However, higher air humidity reduces the exhaust degradation efficiency. The abundant water molecules in the reaction system hinder direct contact between the photocatalyst and the exhaust gas, thereby diminishing photocatalytic activity. Within a relative humidity range of 40% to 80%, photocatalytic performance is significantly affected. Therefore, scholars recommend controlling relative humidity in laboratory tests within 20%~40% [87,88]. Based on this, the photocatalytic reaction system should be a fully sealed reactor equipped with modules for light source, temperature control, humidity control, and a specimen holder. A xenon lamp or UV lamp can serve as the light source, with adjustable light intensity. Temperature and humidity within the reaction system should be dynamically adjustable to simulate actual service environments. The distance between the specimen holder and the light source should be adjustable, and the variation in irradiation intensity along the specimen length must be controlled within ±5%.

Furthermore, in the reaction systems of existing testing devices, the pollutant gas flows steadily over the specimen surface. However, in actual service environments, turbulent flow is generated in the surrounding gas due to vehicle movement, which

reduces the contact efficiency between the pollutant gas and the surface of the photocatalytic fog seal. Therefore, an air-blowing module can be added to the reaction system to simulate the pumping effect induced by vehicle movement.

(3) Testing system

The testing system is used to measure variations in gas concentration within the reaction system. Gas composition analyzers are primarily employed, enabling accurate identification of multiple components in complex gas mixtures and precise determination of the concentration of each component.

Laboratory results should be interpreted with the gap to practical pavement conditions in mind. Laboratory reactors operate at pollutant concentrations of tens to hundreds of ppm, whereas ambient road concentrations are at the ppb level, and laboratory light sources provide ultraviolet intensities far above the solar fraction of about 5%. A systematic review of photocatalytic concrete likewise concluded that laboratory results and field performance differ considerably [89]. Real pavements additionally involve wind, rain washout, dust coverage, tire wear, and aging of the seal under traffic, whereas most reported data were obtained on fresh specimens. Therefore, laboratory screening should be followed by validation in wind tunnels, large-scale test sections, and real roads. Field validation should monitor not only the reduction in pollutant concentration but also the NO_2/NO ratio, conversion products, and the long-term performance of aged seals.

5. Strategies for Enhancing Photocatalytic Performance

At the present stage, the enhancement of the purification efficiency of photocatalytic fog seals is primarily achieved through technical approaches such as element doping, heterostructure construction, and regulation of morphology and structure [6,7,9–11,32,90–94].

5.1. Element Doping

Element doping is a modification technique in which foreign atoms (metals or nonmetals) are introduced into the photocatalyst lattice through physical or chemical methods, creating defects that alter the lattice and electronic structure [95]. The primary purpose of doping is to regulate the band structure—narrowing the band gap to broaden the photoresponse range [96] and to introduce charge trapping centers that promote the separation of photogenerated electrons and holes [97].

At the current stage, the doping elements used in photocatalytic fog seals include nonmetallic elements such as carbon and nitrogen, as well as metallic elements such as Fe [91], Sm [92], Ce [93], and La [98]. A fundamental distinction exists between metal doping and nonmetal doping. Metal doping introduces discrete impurity energy levels into the band gap of the photocatalyst [96], whereas nonmetal doping shifts the valence band position upward, thereby narrowing the band gap [48]. Through metal–nonmetal co-doping, the high electrical conductivity and favorable catalytic activity of metallic elements are combined with the electronegativity and chemical stability of nonmetallic elements, resulting in complex electronic structures and abundant active sites within the material.

Anionic doping with nonmetallic elements, particularly nitrogen, is considered an effective strategy to achieve visible light responsiveness in TiO_2 without compromising its ultraviolet photocatalytic activity [48]. Nitrogen doping narrows the band gap of TiO_2, as evidenced by a red shift in the absorption band observed through UV–Vis diffuse reflectance spectroscopy (DRS) [7]. Activated carbon is a porous carbonaceous material characterized by an exceptionally large specific surface area due to its highly developed

pore structure. This structure facilitates extensive contact with gases, resulting in excellent adsorption performance. Consequently, harmful gases are effectively captured and transferred to the photocatalyst surface, enhancing the catalytic degradation of these gases [90]. However, studies indicate that the photocatalytic reaction can be impeded because activated carbon absorbs the light source, and its synergistic effect with TiO_2 is weaker than the antagonistic effect [9].

In Fe-doped g-C_3N_4, the Fe sites capture the photogenerated electrons and suppress recombination [91]; at excessive doping concentrations, however, the sites become recombination centers and the activity declines. In addition to Fe, Sm-doped TiO_2 (Sm-TiO_2) photocatalysts were prepared via a sol–gel method and applied to waterborne epoxy-modified emulsified asphalt fog seals. A hydrocarbon degradation efficiency of 32% was achieved within 20 min at a spraying rate of 0.118 kg/m^2 [92].

5.2. Heterostructure Construction

To overcome the inherent drawback of rapid recombination of photogenerated electron–hole pairs in single semiconductor photocatalysts, constructing heterojunctions by coupling different semiconductor materials has become a widely adopted modification strategy. Across the heterointerface, electrons and holes migrate in opposite directions, which suppresses their recombination.

Based on this approach, a $Bi_2O_2CO_3$@C_3N_4 heterojunction photocatalyst with visible-light responsiveness was synthesized via a hydrothermal method, and a photocatalytic self-cleaning coating was fabricated using epoxy resin as the film-forming matrix [6]. A NO degradation efficiency of 33% was achieved under visible-light irradiation. In this system, photogenerated electrons transfer from g-C_3N_4 to the conduction band of $Bi_2O_2CO_3$ while the holes remain in the valence band of g-C_3N_4, suppressing recombination; the heterojunction also increases the specific surface area and extends the photoresponse into the visible region [6].

Heterojunctions have also been constructed directly within asphalt systems. A g-C_3N_4/TiO_2 composite, obtained by calcining a melamine and nano TiO_2 mixture, shows TiO_2 particles adhering to the flaky g-C_3N_4, which suppresses agglomeration [99], and removes NO more efficiently than either single component, owing to the heterojunction that accelerates carrier separation [100]. Photocatalytic emulsified asphalt outperformed photocatalytic neat asphalt because the micropores formed during demulsification keep part of the catalyst surface accessible [99], and spraying the catalyst as an aqueous solution outperformed powder spreading at higher dosages because of the better dispersion [100]. The heterojunction thus addresses carrier recombination, while the carrier form and application method determine how much of the gained activity survives in the binder.

5.3. Morphology and Structure Regulation

The catalytic performance of nano photocatalysts can be significantly enhanced through morphology and structural regulation. This improvement is primarily attributed to an increase in specific surface area, enhanced exposure of reactive active sites, improved light absorption, accelerated charge migration, and suppressed carrier recombination [95]. However, nano TiO_2 tends to agglomerate due to its small particle size, which leads to a reduction in specific surface area and a decline in photocatalytic performance. Transforming nano TiO_2 into a three-dimensionally ordered macroporous structure (3DOM TiO_2) effectively suppresses agglomeration within the fog seal. By employing a gel template method using a 5% solution of 300 nm polystyrene microspheres followed by calcination at 550 °C, a 3DOM TiO_2 with a regularly ordered structure can be synthesized [8]. Experimental results demonstrate that the purification capacity of the 3DOM TiO_2 fog seal material, with an optimal pore size of 300 nm, is 15%~25% higher

than that of conventional nano TiO_2 [32]. Furthermore, a photocatalytic fog seal prepared with 2% 3DOM TiO_2 and emulsified asphalt containing 60% solid content achieves a degradation efficiency 42.9% greater than that of a standard nano TiO_2 fog seal at a spraying rate of 0.6 kg/m^2, 28 °C, and 35% relative humidity [8].

5.4. Other Strategies

By loading photocatalytic materials onto carriers with a high specific surface area, catalyst dispersion can be enhanced, exposing more active sites at the reaction interface and thereby effectively improving photocatalytic efficiency. Nano TiO_2 was uniformly deposited onto the surface of glass microspheres using a process involving cold alkali corrosion treatment followed by high-temperature adhesion technology. This method not only improved the dispersion uniformity of nano TiO_2 but also enhanced the light transmittance of the photocatalytic material, resulting in a degradation efficiency 12.5% higher than that of pure nano TiO_2 [10].

When subjected to mechanical stress, piezoelectric materials generate a polarized electric field. This built-in electric field can drive the separation of photogenerated charge carriers, enabling synergistic catalysis by harnessing both the mechanical energy produced by vehicle movement and light energy. A g-C_3N_4/$BaTiO_3$ piezo-photocatalytic fog seal material was developed, effectively reducing the dependence of the photocatalytic fog seal on the light source [11,33]. Particularly under low-light conditions, the band structure of the photocatalytic material shifts due to the potential difference generated by the piezoelectric effect, inducing directional separation and migration of photogenerated charge carriers. These carriers preferentially react with O_2 to generate superoxide radicals, facilitating the degradation of NO. However, the NO degradation efficiency induced by the piezoelectric effect alone is lower than that achieved by pure photocatalysis. Under combined light and traffic loading conditions, the NO degradation efficiency is 139% and 48% higher than under pure piezoelectric and pure photocatalytic conditions, respectively [11,33].

In summary, element doping adjusts the band gap at low cost but may suffer from thermal instability and introduces concerns over dopant toxicity. Heterostructure construction suppresses charge recombination effectively, yet the synthesis is complex and the refined interfaces are vulnerable during field service. Morphology regulation increases the active surface area, but its scale-up to pavement production remains difficult, and noble metal deposition, although highly active, is rarely affordable for fog seals, which are a low-cost preventive maintenance treatment. More importantly, all strategies that raise photocatalytic activity tend to conflict with pavement durability. Increasing the catalyst dosage improves photocatalysis but may weaken the binder and accelerate raveling, whereas a binder-rich surface protects the pavement but buries the catalyst and reduces the active area. Traffic abrasion and dust coverage further erode the surface activity over time. The realistic goal of fog seal design is therefore not the highest photocatalytic activity but the optimum activity under the constraint of pavement durability.

6. Conclusions and Outlook

(1) Photocatalysts currently used in fog seals differ mainly in band structure. Anatase TiO_2 (3.2 eV) and CeO_2 (2.9~3.2 eV) absorb only ultraviolet light, with absorption edges at about 387 nm and 380~420 nm, respectively. g-C_3N_4 (about 2.7 eV, edge about 460 nm) and $ZnIn_2S_4$ (2.06~2.85 eV) extend the response into the visible region, but the former suffers from rapid carrier recombination and the latter from photocorrosion. Since the reported specific surface areas span 10 to 213 m^2/g, the activity difference cannot be explained by surface area alone. For a fog seal, the more

important factor is the proportion of catalyst surface that remains exposed after the binder has cured. Asphalt films covering the particles or filling the pores reduce the degradation efficiency considerably, but this embedding effect is not reflected by the optical or structural indicators used for powder characterization, and it has not been quantitatively evaluated in the existing studies.

(2) The performance data reported in the literature are not yet comparable. Among the existing testing devices, the reactor volume varies from 27 to 676 L, the light intensity from 8.9~300 W/m^2, and the initial NO concentration spans more than four orders of magnitude, from the ppb level to several hundred ppm. Under such different conditions, the reported degradation efficiencies cannot be directly compared. The improvements reported for the enhancement strategies were likewise obtained under different conditions. These values reflect the level of improvement that can be achieved, but they cannot be used as a basis for ranking the modification methods. Element doping and heterostructure construction narrow the band gap or suppress carrier recombination, morphology regulation enlarges the active surface, and noble metal deposition promotes charge separation, while loading on carriers such as glass microspheres improves the retention of the catalyst on the pavement. Each route, however, pays a price in complexity, stability or cost, and none has been assessed under traffic, aging and abrasion.

(3) Three aspects should be emphasized in subsequent research. First, a fog seal binder should be designed for the photocatalytic function, leaving part of the catalyst surface exposed, and the embedding effect should be quantified through the efficiency per unit of exposed area, surface Ti/Si mapping or XPS, and the light transmittance of the cured film. Second, a unified testing procedure should be established, with a sealed reactor, an initial NO concentration of 0.5~1.0 ppm, a relative humidity of 20%~40%, and an irradiance of 30 W/m^2 with no more than ±5% variation, together with the conversion rate, NO_2 yield and nitrate mass balance. Third, durability should be expressed as the retention of activity, evidenced by the activity remaining after a specified abrasion sequence and by field sections monitored for at least twelve months against unsealed controls, on which basis the cost per unit of NOx removed can be assessed.

Author Contributions: Z.F.: Conceptualization, Investigation, Data Curation, Formal Analysis, Writing—Original Draft; R.Z.: Investigation, Data Curation, Writing—Original Draft; Q.C.: Conceptualization, Methodology, Supervision, Funding Acquisition, Writing—Review & Editing; F.X.: Visualization, Investigation; C.X.: Project Administration. All authors have read and agreed to the published version of the manuscript.

Funding: This research was funded by the Shandong Postdoctoral Science Foundation, grant number SDZZ-ZR-202601026.

Institutional Review Board Statement: Not applicable.

Informed Consent Statement: Not applicable.

Data Availability Statement: No new data were created or analyzed in this study. Data sharing is not applicable to this article.

Conflicts of Interest: Authors Zhentong Fan, Renjie Zhu and Futong Xu were employed by the company the Second Construction Limited Company of China Construction Eighth Engineering Division; Author Chaozhen Xue was employed by the company Shandong Zhongjian Engineering Quality Inspection Co., Ltd. The remaining author declare that the research was conducted in the absence of any commercial or financial relationships that could be construed as potential conflicts of interest.

Abbreviations

The following abbreviations are used in this manuscript:

UV-Vis	Ultraviolet-visible spectroscopy
CNT-ZIS	Carbon Nanotube-$ZnIn_2S_4$
3DOM	Three-dimensionally ordered macroporous
PPC-SFS	Piezo-photocatalytic sand fog seal

References

1. Ministry of Ecology and Environment of the People's Republic of China. *China Mobile Source Environmental Management Annual Report (2025)*; Ministry of Ecology and Environment: Beijing, China, 2025.
2. Editorial Department of China Journal of Highway and Transport. Review on China's pavement engineering research: 2024. *China J. Highw. Transp.* **2024**, *37*, 1–81.
3. Guo, M.; Zhang, R.; Du, X.L.; Liu, P.F. A state-of-the-art review on the functionality of ultra-thin overlays towards a future low carbon road maintenance. *Engineering.* **2024**, *32*, 82–98.
4. Ui Abadeen, A.Z.; Omranian, S.R.; Bolm, J.; Den Bergh, S.V.; Zhang, H.P.; Verbruggen, S.W.; Vuye, C. Influence of inlet concentration, UV intensity, and relative humidity on NOx degradation in photocatalytic asphalt pavement. *Road Mater. Pavement Des.* **2025**, 1–20.
5. Yan, S.J.; Wang, Y.Y.; Chi, F.X.; Luo, X.; Zhang, T.J.; Xi, C. Study on air-purifying performance of semi-flexible asphalt samples coated with titanium dioxide using different methods. *J. Renew. Mater.* **2022**, *10*, 1321–1335.
6. Xia, H.Y.; Wu, Z.L.; Li, J.J.; Yan, M.; Song, L.; Cui, L.Y. Preparation and performance of $Bi_2O_2CO_3$@C_3N_4-PFDTES/EP self-cleaning synergistic photocatalytic coating. *Acta Mater. Compos. Sin.* **2026**, *43*, 2232–2244.
7. Zhang, L.; Lu, Q.; Shan, R.; Zhang, F.L.; Muhammad, Y.; Huang, K. Photocatalytic degradation of vehicular exhaust by nitrogen-doped titanium dioxide modified pavement material. *Transp. Res. Part D Transp. Environ.* **2021**, *91*, 102690.
8. Xu, L.; Wang, Z.; Dai, Y.; Wu, L.; Ye, X.; Xu, S.F. Performance of a 3DOM TiO_2 fog seal layer in degrading nox from vehicle exhaust. *J. Mater. Civ. Eng.* **2025**, *37*, 04024499.
9. He, C.; Xiao, Q.; Gong, F.; Yang, Y.; Ren, X. Functional materials based on active carbon and titanium dioxide in fog seal. *Mater.* **2020**, *13*, 5267.
10. Pan, H.; Chen, X.S.; Wang, L.; Mei, Y.; Xu, D.M. Photocatalytic performance and economy of de-NOx in urban tunnel exhaust by TiO_2. *China Environ. Sci.* **2019**, *39*, 118–125.
11. Liu, G.; Zhao, T.; Wu, J.; Chang, M.; Fei, H.; Yang, S.Q.; Li, Q. Enhanced removal and selective conversion for NO with N-vacancies g-C3N4\BaTiO3 by piezo-photocatalysis. *Sep. Purif. Technol*. 2025, 360, 1: 130914.
12. Guo, T.T.; Chen, Y.Z.; Fang, C.Z.; Li, Z.X.; Li, D.; He, Q.Y.; Chen, H.J. Preparation and performance of environmentally friendly micro-surfacing for degradable automobile exhaust gas. *Polymers.* **2025**, *17*, 760.
13. Guo, L.Y.; Xu, S.F.; Huang, Y.Y.; Xu, Y. Effect evaluation of automobile exhaust decomposition by using fog seal containing nano-TiO_2. *J. Beijing Univ. Civ. Eng. Archit.* **2017**, *33*, 27–32.
14. Liu, Z.M.; Jia, X.; Peng, J.L.; Yang, C.; Liu, C. Evaluation of construction and tail gas degradation efficiency of photocatalytic sand-fog sealing layer based on entity engineering. *MR* **2025**, *39*, 143–149.
15. Tang, S.C.; Mu, B.H.; Li, Y.J.; Li, Y.; Cao, Y.; Bahnemann, D.; Pan, J. Advances in TiO_2-enhanced photocatalytic building materials: Applications in cement and asphalt for environmental purification. *Low Carbon Mater. Green Constr.* **2024**, *2*, 26.
16. Hu, C.; Ma, J.; Jiang, H.; Chen, Z.; Zhao, J. Evaluation of nano-TiO_2 modified waterborne epoxy resin as fog seal and exhaust degradation material in asphalt pavement. *J. Test. Eval.* **2017**, *45*, 260–267.
17. Segundo, I.R.; Landi, S.; Margaritis, A.; Pinpintakos, G.; Freiats, E.; Vuye, C.; Blom, J.; Tytgat, T.; Denys, S.; Carneiro, J. Physicochemical and rheological properties of a transparent asphalt binder modified with Nano-TiO_2. *Nanomaterials* **2020**, *10*, 2152.
18. Qian, G.P.; Yu, H.N.; Gong, X.B.; Zhao, L. Impact of Nano-TiO_2 on the NO_2 degradation and rheological performance of asphalt pavement. *Constr. Build. Mater.* **2019**, *218*, 53–63.
19. Ma, Y.Z.; Li, L.L.; Wang, H.; Wang, W.; Zheng, K. Laboratory Study on performance evaluation and automobile exhaust degradation of nano-TiO_2 particles-modified asphalt materials. *Adv. Mater. Sci. Eng.* **2021**, *2021*, 5574013.

20. Wu, H.S.; Shen, A.Q.; Yang, X.L.; He, Z.M.; Zhang, Y.H. Effect of TiO_2/CeO_2 on photocatalytic degradation capability and pavement performance of asphalt mixture with steel slag. *J. Mater. Civ. Eng.* **2021**, *33*, 04021234.
21. Li, Y. Study on the NO degradation performance of a nanomaterial fog seal. Master's thesis, Changsha University of Science and Technology, Changsha, China, 2015.
22. Zhao, D.; Wu, X.; Gu, X.Y.; Liu, J. Investigation into the degradation of air and runoff pollutants using nano g-C_3N_4 photocatalytic road surfaces. *Constr. Build. Mater.* **2024**, *411*, 134553.
23. Wang, Y.; Wang, X.Y.; Niu, D.Y.; Niu, Y.H.; Xia, H.Y.; Wang, Y. Effect of photocatalyst on rheological behavior and no degradation capacity of asphalt binder. *Catalysts.* **2023**, *13*, 1083.
24. Zhang, W.K. Study on the Preparation, Performance, and application of CNT-$ZnIn_2S_4$ composite photocatalytic materials for road use. Master's thesis, Shandong Jiaotong University, Jinan, China, 2024.
25. Cao, X.J.; Deng, M.; Tang, B.M.; Ding, Y.; Yang, X. Development of photocatalytic chip seal for nitric oxide removal on the surface of pavement using g-C_3N_4/TiO_2 composite. *Road Mater. Pavement.* **2019**, *22*, 1178–1194.
26. Huang, Y.; Zhang, J.; Wang, Z.Y.; Liu, Y.; Wang, P.; Cao, J.J.; Ho, W. G-C_3N_4/TiO_2 Composite film in the fabrication of a photocatalytic air-purifying pavements. *Sol. RRL.* **2020**, *4*, 2000170.
27. Zeng, C.; Deng, M.; Qian, H.; Tang, B.; Ding, Y.; Cao, X.J. Movable plates with g-C_3N_4/TiO_2 as a compound system for a greener urban parking lot environment. *PLoS ONE.* **2020**, *15*, e0231286.
28. Xu, P.; Yan, X.L.; Ge, J.G.; Cai, J.; Qian, G.; Yu, H.; Gu, F. Research on the preparation of composite BOCN-TiO_2 photocatalytic materials and their exhaust gas degradation in road domains. *Constr. Build. Mater.* **2025**, *494*, 143584.
29. Fan, W.G.; Chan, K.Y.; Zhang, C.X.; Zhang, K.; Ning, Z.; Leung, M.K.H. Solar photocatalytic asphalt for removal of vehicular NOx: A feasibility study. *Appl. Energ.* **2018**, *225*, 535–541.
30. Shan, B.L.; Cao, X.J.; Yang, X.Y.; Shang, T.; Ding, Y.; Tang, B. Highly active photocatalytic asphalt pavement for NOx removal using iron-doped g-C_3N_4. *Road Mater. Pavement.* **2022**, *23*, 2531–2546.
31. Cui, S.C.; Cheng, R.; Sun, F.; Zhao, H.S.; Yuan, H.; Si, Q.; Ai, M.Z.; Du, W.; Zhou, K.; Duan, Y.; et al. G-$C_3N_4/CeO_2/Bi_2O_3$ dual type-II heterojunction photocatalysis self-cleaning coatings: From spectral absorption modulation to engineering application characterization. *Nanomaterials.* **2025**, *16*, 16.
32. Xu, Y.; Li, X.; Duan, M.; Fan, Z.Q.; Wang, Z.H.; Xu, S.F.; Liu, H. Performance study of 3DOM TiO_2 fog seal material for photocatalytic degradation of NO in vehicle exhaust. *J. Mater. Civ. Eng.* **2023**, *35*, 04023432.
33. Liu, G.Y.; Zhao, T.Z.; Wu, J.Y.; Zhan, Y.B.; Kuang, M.C.; Run, M.T.; Li, F.; Yang, S.Q. Piezo-photocatalytic NO degradation performance and load-light coupling mechanism of g-$C_3N_4/BaTiO_3$ fog seal pavements. *Chem. Eng. J.* **2025**, *517*, 164405.
34. Jin, J.; Xiao, T.; Tan, Y.Q.; Zheng, J.; Liu, R.; Qian, G.; Wei, H.; Zhang, J.H. Effects of TiO_2 pillared montmorillonite nanocomposites on the properties of asphalt with exhaust catalytic capacity. *J. Clean. Prod.* **2018**, *205*, 339–349.
35. Ayar, P.; Ruhi, A.; Baibordy, A.; Azadgoleh, M.A.; Mohammadi, M.M.; Abdipour, S.V. Toward sustainable roads: A critical review on nano-TiO_2 application in asphalt pavement. *Innov. Infrastruct. Solut.* **2024**, *9*, 148.
36. Wang, C.H.; Fan, Z.T.; Wang, Z.B.; Li, Y.W.; Feng, L.; Tan, S.Y. Fog seal with polymer composite modified emulsified asphalt: Road performance and environmental adaptability. *Wear* **2025**, *562*, 205672.
37. Wang, C.H.; Fan, Z.T.; Chen, Q.; Song, L. Seepage characteristics and multi-scale evaluation of resin-based seepage-solidified fog seal materials for asphalt pavements. *J. Traffic. Transp. Eng.* **2026**, 1–21. https://doi.org/10.19818/j.cnki.1671-1637.2026.182.
38. Chen, Q.; Wang, J.L.; Song, L.; Fan, Z.T.; Wang, C.H. Sustainable resin-based fog seal materials replacing asphalt: Design of high penetrability, bond strength and aging resistance toward cleaner pavement maintenance. *Case Stud. Constr. Mat.* **2026**, *24*, e06204.
39. Wang, C.H.; Fan, Z.T.; Wang, Z.B.; Yu, J.; Chen, Q.; Fu, H. Multi-component waterborne polymer modifiers for road emulsified asphalt: Modular design, mechanism of action and performance evaluation. *J. Clean. Prod.* **2025**, *513*, 145740.
40. Fan, Z.T.; Wang, C.H.; Li, Y.W.; Feng, L.; Chen, Q. State of the art review on fog seal for asphalt pavement: Material composition, classification, performance evaluation, and mechanism analysis. *Prog. Org. Coat.* **2024**, *194*, 108573.
41. Wang, D.Y.; Zheng, X.Y. Research on the effect of nano TiO_2 on the properties of emulsified asphalt and its purification performance. *Highway.* **2022**, *67*, 310–315.
42. Segundo, I.C.D.; Dias, E.A.L.; Fernandes, F.D.P.; de Freitas, E.F.; Costa, M.F.; Carneiro, J.O. Photocatalytic asphalt pavement: The physicochemical and rheological impact of TiO_2 nano/microparticles and ZnO microparticles onto the bitumen. *Road Mater. Pavement.* **2019**, *20*, 1452–1467.
43. Jia, X.; Li, J.T.; Niu, Z.Y.; Wang, Y.; Meng, Z.; Wang, X. TiO_2-modified emulsified asphalt exhibits enhanced high-temperature performance and photocatalytic functionality. *Coatings.* **2026**, *16*, 532.

44. Cadorin, N.D.; de Melo, J.V.S.; Broering, W.B.; Manfor, A.L.; Barra, B.S. Asphalt nanocomposite with titanium dioxide: Mechanical, rheological and photoactivity performance. *Constr. Build. Mater.* **2021**, *289*, 123178.
45. Albayati, A.H.; Oukaili, N.K.; Moudhafar, M.M.; Allawi, A.A.; Said, A.I.; Ibrahim, T.H. Experimental Study to Investigate the Performance-Related Properties of Modified Asphalt Concrete Using Nanomaterials Al_2O_3, SiO_2, and TiO_2. *Materials.* **2024**, *17*, 4279.
46. Segundo, I.G.D.; Landi, S.; Oliveria, S.M.B.; de Freitas, E.F.; Carneiro, J.A.O. Photocatalytic asphalt mixtures: Mechanical performance and impacts of traffic and weathering abrasion on photocatalytic efficiency. *Catal. Today.* **2019**, *326*, 94–100.
47. Nagaraj, K.; Radha, S.; Deepa, C.G.; Raja, K.; Umapathy, V.; Badgujar, N.P.; Parekh, N.M.; Manimegalai, T.; Devi, L.A.; Uhtra, C. Photocatalytic advancements and applications of titanium dioxide (TiO_2): Progress in biomedical, environmental, and energy sustainability. *Next Res.* **2025**, *2*, 100180.
48. Wang, L.; Chen, Y.; Zhao, H.; Han, B.; Sun, R.M. Advances in nonmetal-doped titanium dioxide photocatalysts. *MR.* **2015**, *29*, 147–151.
49. Zhang, G.; Wu, H.; Chen, D.; Li, N.; Xu, Q.; Li, H.; He, J.; Lu, J. A mini-review on $ZnIn_2S_4$-Based photocatalysts for energy and environmental application. *Green Energy Environ.* **2022**, *7*, 176–204.
50. Li, M.; Zhao, Z.; Li, H.; Wang, Y.; Wang, Q.; Zhu, X.; Fan, L. Study on engineering application and degradation efficiency of nanoscaled TiO_2 used as photocatalytic fog sealing. *Adv. Mater. Sci. Eng.* **2021**, *2021*, 1379886.
51. Huang, X.; Zhang, K.; Peng, B.; Wang, G.; Martin, M.; Wang, F. Ceria-based materials for thermocatalytic and photocatalytic organic synthesis. *ACS Catal.* **2021**, *11*, 9618–9678.
52. Jia, T.; Luo, F.; Chu, F.; Xiao, Y.; Liu, Q.; Pan, W.; Li, F. Nanosized Zn-In spinel-type sulfides loaded on facet-oriented CeO_2 nanorods heterostructures as Z-scheme photocatalysts for efficient elemental mercury removal. *Sci. Total Environ.* **2022**, *813*, 151865.
53. Miao, K.; Li, S.; Zhang, Y.; Liu, Q.; Wu, Y.; Liu, P.; Xu, H.; Le, S.; Zhu, C. Recent progress of modified CeO_2-based materials for photocatalytic environmental remediation and antibacterial activity. *Environ. Funct. Mater.* **2023**, *2*, 213–227.
54. Yan, Y.Q.; Wu, Y.Z.; Wu, Y.H.; Weng, Z.L.; Liu, S.J.; Liu, Z.G.; Lu, K.Q.; Han, B. Recent advances of CeO_2-based composite materials for photocatalytic applications. *ChemSusChem* **2024**, *17*, e20230177.
55. Zhou, D.; Zhai, P.; Hu, G.; Yang, J. Upconversion luminescence and enhanced photocatalytic hydrogen production for Er^{3+} doped $SrTiO_3$ nanopaeticles. *Chem. Phys. Lett.* **2018**, *711*, 77–80.
56. Zhou, J.; Shi, X.H.; Wang, L. Research progress on synthesis and application of $SrTiO_3$. *New Chem. Mater.* **2026**, *54*, 60–65.
57. He, Z.; Sun, X.Y.; Gu, X. $SrTiO_3$ nanoparticles and nanofibers: Synthesis and comparison of photocatalytic properties. *J. Mater. Sci. Mater. Electron.* **2017**, *28*, 13950–13955.
58. Su, R.J.; Liang, H.R.; Jiang, H. Research status and application prospect of g-C_3N_4. *Appl. Chem. Ind.* **2025**, *54*, 2993–2999.
59. Li, M.Y.; Yang, L.Q.; Song, Y.Z.; Hou, H.; Fang, Y.; Liu, Y.; Xie, L.; Lu, D. Research progress on the preparation, modification, and applications of g-C_3N_4 in photocatalysis and piezoelectric photocatalysis. *Inorganics* **2025**, *13*, 300.
60. Xiao, Z.; Do, H.; Yusuf, A.; Ma, H.; Jiang, S.; Li, J.; Sun, Y.; Wang, C.; Ren, Y.; Chen, G.; et al. Facile synthesis of multi-layer $Co(OH)_2$/CeO_2-g-C_3N_4 ternary synergistic heterostructure for efficient photocatalytic oxidation of NO under visible light. *J. Hazard. Mater.* **2024**, *462*, 132744.
61. Wang, W.; Li, B.; Shi, J.; Zh, K.; Liu, X.; Li, C.; Hu, F.Y.; Xi, X.G.; Kawi, S. High-efficiency photocatalytic hydrogen and oxygen evolution properties by Z-scheme electron transfer in $BiVO_4$/C_3N_5 heterostructure. *Appl. Catal. B Environ. Energy* **2025**, *362*, 124766.
62. Xing, J.; Huang, X.; Yong, X.; Li, X.; Wang, J.K.; Wang, N.; Hao, H.X. N-doped synergistic porous thin-walled g-C_3N_4 nanotubes for efficient tetracycline photodegradation. *Chem. Eng. J.* **2023**, *455*, 140570.
63. Wei, H.N.; Li, J.J.; Sheng, J.C. Research progress on modification of graphite phase carbon nitride photo catalyst. *Mater. Sci.* **2021**, *11*, 1271–1283.
64. Zhang, M.; Yang, Y.; An, X.; Hou, L. A critical review of g-C_3N_4-based photocatalytic membrane for water purification. *Chem. Eng. J.* **2021**, *412*, 128663.
65. Gaurav, Y.; Ahmaruzzaman, M. Q $ZnIn_2S_4$ and $ZnIn_2S_4$ based advanced hybrid materials: Structure, morphology and applications in environment and energy. *Inorg. Chem. Commun.* **2022**, *138*, 109288.
66. Zhu, M.; Zhang, F.; Wang, Y.; Meng, Z.D.; Mi, C.Q. Preparation and photocatalytic hydrogen evolution performance of square platform Cu_2MoS_4/lamellar $ZnIn_2S_4$. *React. Chem. Eng.* **2023**, *8*, 933–942.
67. Pan, Y.; Yuan, X.; Jiang, L.; Yu, H.B.; Zhang, J.; Wang, H.; Guan, R.P.; Zeng, G.M. Recent advances in synthesis, modification and photocatalytic applications of micro/nano-structured zinc indium sulfide. *Chem. Eng. J.* **2018**, *354*, 407–413.

68. Wang, J.; Sun, S.; Zhou, R.; Li, Y.Z.; He, Z.T.; Ding, H.; Chen, D.M.; Ao, W.H. A review: Synthesis, modification and photocatalytic applications of $ZnIn_2S_4$. *J. Mater. Sci. Technol.* **2021**, *78*, 1–19.
69. Xia, Y.; Li, Q.; Lv, K.; Li, M. Heterojunction construction between TiO_2 hollowsphere and $ZnIn_2S_4$ flower for photocatalysis application. *Appl. Surf. Sci.* **2017**, *398*, 81–88.
70. Zheng, X.; Song, Y.; Liu, Y.; Yang, Y.; Wu, D.X.; Yang, Y.J.; Feng, S.Y.; Li, J.; Liu, W.F.; Shen, Y.J.; et al. $ZnIn_2S_4$-based photocatalysts for photocatalytic hydrogen evolution via water splitting. *Coord. Chem. Rev.* **2023**, *475*, 2148989.
71. Zhang, Y.; Wang, Y.; Wu, X.; Li, T.; Zhao, F.L.; Tan, J.; Liu, M.; Huang, H.W. Photocorrosion of metal sulfides: Mechanism, characterization, anti-photocorrosion strategies and solar catalysis applications. *Coord. Chem. Rev.* **2025**, *545*, 217021.
72. Lee, J.W.; Baek, C. Evaluation of NOx reduction effect and impact on asphalt pavement of surface treatment technology including TiO_2 and asphalt rejuvenator. *Appl. Sci.* **2021**, *11*, 11571.
73. Wu, P.; Wang, X.C. Purification performance of thin layer cover of TiO_2 modified asphalt. *J. Jiangsu Univ. Nat. Sci. Ed.* **2017**, *38*, 113–118.
74. Xu, S.F.; Li, S.T.; Li, S.F.; Li, Z.; Li, J.Z.; Niu, Y.J. Development and evaluation of stabilizer for automobile exhaust gas degradation materials application in pavement. *China J. Highw. Transp.* **2019**, *32*, 114–121.
75. Huang, C.Y.; Liu, C.B.; Zheng, L.Z.; Qiu, Y.; Meng, X.; Chen, Z. Research progress for the controlled synthesis and photocatalytic performance of deep-coloredgraphitic carbon nitride. *Acta Mater. Compos. Sin.* **2026**, *43*, 3421–3441.
76. Cao, X.J.; Liu, Y.G.; Liu, X.F.; Liu, P.; Guo, P. First-principles calculation and photocatalytic property evaluation of rare earth Sm doped TiO_2. *New Chem. Mater.* **2019**, *47*, 180–184.
77. Shan, R. Research on modification of titanium dioxide photocatalytictail gas degradation pavement material. Master's thesis, Southeast University, Nanjing, China, 2018.
78. Wang, T. Full Aging degradation of exhaust gas fog sealing layer performance research and technology application. Master's thesis, Hebei University of Engineering, Shijiazhuang, China, 2023.
79. Wang, Z.H. Improvement of NO degradation performance of TiO_2-based photocatalyst mist coating material. Master's thesis, Beijing University of Civil Engineering and Architecture, Beijing, China, 2024.
80. Zhang, W.G.; Wang, F.; Li, Z.M. A study on preparation of automobile exhaust decomposition type pavement material and relationship with irradiance. *Sci. Technol. Eng.* **2017**, *17*, 298–301.
81. Yan, S.J.; Wang, Y.Y.; Chi, F.X.; Luo, X. Characterization and synthesis of hollow glass microspheres/nano-TiO_2 composite material. *J. Zhejiang Univ. Eng. Sci.* **2021**, *55*, 713–719.
82. Guo, Y.C.; Xie, Z.T.; Shen, A.Q.; Zhang, Y.H. Research on tunnel tail gas degradation of coated composite nano-photocatalytic materials. *Bull. Chin. Ceram. Soc.* **2019**, *38*, 2563–2569.
83. Yuan, G.Y. Development and evaluation of TiO_2-based auto exhaust degradationasphalt pavement material. Beijing University of Civil Engineering and Architecture, Beijing, China, 2016.
84. Li, W.B. Research of photocatalytic decomposition titainum dioxide on asphalt pavement. Master's thesis, Xinjiang University, Urumqi, China, 2017.
85. Huang, M.; Wen, X.J. Experimental study on photocatalytic effect of nano TiO_2 epoxy emulsified asphalt mixture. *Appl. Sci.* **2019**, *9*, 2464.
86. Wang, H.; Jin, K.; Dong, X.Y.; Zhan, C.; Liu, C. Preparation technique and properties of nano-TiO_2 photocatalytic coatings for asphalt pavement. *Appl. Sci.* **2018**, *8*, 2049.
87. Guo, Y.M.; Wu, F.; Hong, X.Y.; Zhou, X.; Wu, L. Experimental study on automobile exhaust gas degradation performance of photocatalytic pavement material. *Sci. Technol. Eng.* **2018**, *18*, 268–272.
88. Casagrande, C.A.; Repette, W.L.; Hotza, D. Effect of environmental conditions on degradation of NOx gases by photocatalytic nanotitania-based cement mortars after long-term hydration. *J. Clean Prod.* **2020**, *274*, 123067.
89. Chouohan, J.; Chandrappa, A.K. A systematic review on photocatalytic concrete for pavement applications: An innovative solution to reduce air pollution. *Innov. Infrastruct. Solut.* **2023**, *8*, 90.
90. Varnagiris, S.; Medvids, A.; Lelis, M.; Milcius, D.; Antuzevics, A. Black carbon-doped TiO_2 films: Synthesis, characterization and photocatalysis. *J. Photochem. Photobiol. A Chem.* **2019**, *382*, 111941.
91. Cao, X.J.; Shan, B.L.; Deng, M.; Tang, B. Preparation and photocatalytic properties of Fe-doped g-C_3N_4 photocatalyst. *J. Chongqing Jiaotong Univ. Nat. Sci.* **2019**, *38*, 52–57.
92. Sun, F.; Zhang, X.K.; Jia, X.D. Application of Sm-TiO_2 fog sealing material in degradation of automobile exhaust. *New Chem. Mater.* **2019**, *47*, 213–216.

93. Cao, X.; Yang, X.; Li, H.; Huang, W.; Liu, X.F. Investigation of Ce-TiO_2 photocatalyst and its application in asphalt-based specimens for NO degradation. *Constr. Build. Mater.* **2017**, *148*, 824–832.
94. Liu, G.Y. Preparation, properties and mechanism of high efficiency photocatalytic degradation no coating on tunnel inner wall. Master's thesis, Chang'an University, Xi'an, China, 2022.
95. Li, G.Q.; Liang, H.O.; Li, C.P.; Bai, J. Research progress on preparation and modification of $ZnIn_2S_4$-based photocatalyst. *MR.* **2024**, *38*, 11–16.
96. Li, D.Y.; Zhang, W.T.; Zhang, C. Research progress in improving the photocatalytic properties of TiO_2 materials by doping with different metals. *MR.* **2019**, *33*, 3900–3907.
97. Peiris, S.; de Silva, H.B.; Ranasing, K.N.; Bandara, S.V.; Perera, I.R. Recent development and future prospects of TiO_2 photocatalysis. *J. Chin. Chem. Soc.* **2021**, *68*, 738–769.
98. Tang, B.M.; Liu, X.F.; Huang, W.; Cao, X.J. Preparation of La-doped nanometer TiO_2 and its application for NO removal on asphalt concrete. *Road. Mater. Pavement Des.* **2017**, *18*, 43–53.
99. Cao, X.J.; Yang, X.Y.; Wu, T. G-C_3N_4/TiO_2 photocatalyst and its performance of NO degradation in emulsified asphalt. *J. Mater. Civ. Eng.* **2019**, *31*, 04019031.
100. Yang, X.Y.; Tang, B.M.; Wu, T. G-C_3N_4/TiO_2 Composite photocatalyst and its application to asphalt for NO removal. *J. Mater. Civ. Eng.* **2019**, *31*, 04019141.

Disclaimer/Publisher's Note: The statements, opinions and data contained in all publications are solely those of the individual author(s) and contributor(s) and not of MDPI and/or the editor(s). MDPI and/or the editor(s) disclaim responsibility for any injury to people or property resulting from any ideas, methods, instructions or products referred to in the content.